ADVANCED MATERIALS
www.advmat.de

All-in-Fiber Chemical Sensing

*Alexander Gumennik, Alexander M. Stolyarov, Brent R. Schell, Chong Hou, Guillaume Lestoquoy, Fabien Sorin, William McDaniel, Aimee Rose, John D. Joannopoulos, and Yoel Fink**

Optical fibers have been actively investigated for remote chemical sensing applications.[1–17] Luminescence-based detection schemes[18–22] are of particular interest for detection of hazardous materials, such as explosives, where optical fibers are used for collecting and transmitting an emissive signal to a detector at the fiber end. Inherent to this approach are several limitations. First, the standoff distance and sensitivity of detection are restricted by the fiber's numerical aperture (NA), its transmission and bending losses, and the sensitivity of the detector. While the NA can be increased with hollow core photonic bandgap fibers[15,17] and highly sensitive photodetectors can be implemented, limitations on coupling efficiency and propagation losses present challenges to distributed sensing over large areas.

Here, we introduce and demonstrate an approach for remote luminescence-based chemical detection that is inherently adaptable for distributed sensing and circumvents the aforementioned limitations. Rather than rely on the propagation of the optical signal to a distal external detector, we monolithically realize the photodetecting function as an integral part of the fiber itself along its entire length. This approach maximizes signal collection efficiency, while eliminating the need to propagate the optical signal along the fiber. Previously reported metal-semiconductor-metal photodetecting fibers[23–26] were characterized under relatively high incident power (mW scale); however, their high noise equivalent power (NEP) precluded their use for chemiluminescent (CL) sensing applications, which require the detection of radiation at the nW scale. By designing and optimizing the fiber materials and architecture for chemical sensing, we succeeded in reducing the NEP by nearly two orders of magnitude compared to previous work.[24] Consequently, we demonstrate trace-level detection limits of peroxide vapor down to 10 parts per billion (ppb), on par with current state-of-the-art hydrogen peroxide vapor sensors, that hitherto have been developed only for non-remote detection.[21,22] Liquid peroxide-based explosives (PBE) have emerged as materials of choice for makeshift explosives. Indeed PBE have been used in a number of recent incidents involving bombing of mass transit systems,[27] leading to world-wide restrictions on liquids carried on board aircraft that is still enforced today. The small footprint, potential for multiplexing, flexible form factor, scalable manufacturing, and compatibility with miniaturized electronics of the fiber architectures demonstrated here enable remote and distributed sensing schemes to meet current societal needs.

The design of the fiber structure dictates its detection capabilities. First, the azimuthal numerical aperture of the detectors should be maximized in order to collect as much of the isotropically emitted CL detection signal as possible. Second, the chosen chalcogenide glass should absorb at the detection wavelength, while remaining thermomechanically compatible for drawing with the other materials comprising the preform. The central wavelength emitted by the peroxide sensing material is 532 nm,[17] which makes crystalline $Se_{97}S_3$ (E_g = 1.74 eV)[28] a suitable candidate. This glass can be codrawn in its amorphous state with polysulfone (PSU) and crystalized post-draw, which makes PSU a good candidate for the polymer cladding material.[29,30] Third, in order to be detectable, the small photocurrent signal resulting from the CL emission must be greater than the noise current level. For weak signals, this noise is proportional to the square root of the dark current,[31] which should therefore be minimized to enhance the signal-to-noise ratio (SNR). Consequently, the appropriate geometry of the $Se_{97}S_3$ layer should be implemented.[24] Note also that if n identical photodetectors are connected in parallel, both I_{bright} and I_{dark} scale linearly with n. However, the noise only grows as $\sqrt{I_{dark}} \propto \sqrt{n}$, while the signal $I_{bright} - I_{dark}$ grows as n, and therefore the SNR scales as $\sqrt{n}$, which is an incentive to integrate multiple independent detectors into one fiber.

Taking into account the above design considerations, a hollow core rectangular preform was assembled and thermally

Dr. A. Gumennik, Dr. A. M. Stolyarov, C. Hou, G. Lestoquoy, Dr. F. Sorin, Prof. J. D. Joannopoulos, Prof. Y. Fink
Research Laboratory of Electronics
MIT, Cambridge, MA 02139, USA
E-mail: yoel@mit.edu
Dr. A. Gumennik, Dr. A. M. Stolyarov, C. Hou, G. Lestoquoy, Dr. F. Sorin, Prof. J. D. Joannopoulos, Prof. Y. Fink
Institute for Soldier Nanotechnologies
MIT, Cambridge, MA 0213, USA
B. R. Schell, W. McDaniel, Dr. A. Rose
FLIR Systems, North Billerica, MA 01862, USA
G. Lestoquoy
Department of Electrical Engineering and Computer Science
MIT, Cambridge, MA 02139, USA
Dr. F. Sorin
Laboratoire Surface du Verre et Interfaces
Unité Mixte CNRS/Saint-Gobain UMR 125
39 quai Lucien Lefranc, 93303 Aubervilliers, France
Prof. J. D. Joannopoulos
Department of Physics
MIT, Cambridge, MA 02139, USA

DOI: 10.1002/adma.201203053

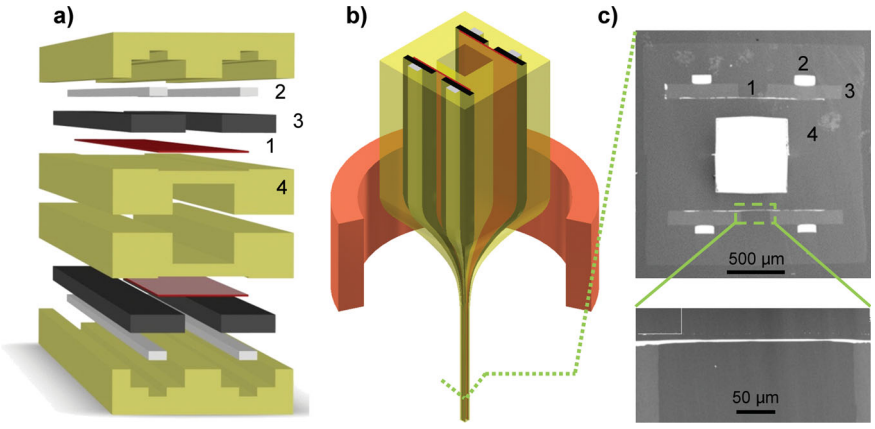

Figure 1. Fiber fabrication process: a) Schematic of the preform assembly. (1) Thin PSU sheet (75 μm) with $Se_{97}S_3$ layer (35 μm) evaporated onto its laminar facet. (2) $Sn_{63}Pb_{37}$ electrodes and (3) CPC pads are incorporated in between (4) PSU plates, which are machined to encapsulate all of the components. The assembly is then thermally consolidated to form a monolithic macroscopic preform. b) Schematics of the thermal drawing process showing the preform fed through the hot zone of a furnace (red ring) and drawn into a fiber. c) Cross sectional SEM micrograph of the resulting fiber. (1) $Se_{97}S_3$ layer, (2) $Sn_{63}Pb_{37}$ electrodes, (3) CPC pads, (4) PSU matrix.

consolidated under vacuum at ≈225 °C as shown in **Figure 1**a. In this design, two identical independent photodetecting structures were incorporated into the preform to demonstrate the aforementioned sensitivity enhancement. The aspect ratio for each of the photoconductive channels was maximized in order to increase the azimuthal numerical aperture while decreasing the dark conductance of each detector, which scales inversely with the layer thickness.[24]

Additional preform materials design constraints emerge from the fact that drawing a thin and wide $Se_{97}S_3$ sheet is complicated by its tendency to undergo capillary break up into thin filaments while being thermally drawn.[29,30] We found that controlling the surface roughness of the preform materials surrounding the $Se_{97}S_3$ layer was key to maintaining its continuity during the draw. Thus, the preform is designed in such a way that only laminar polymer surfaces are in contact with the $Se_{97}S_3$ layer. Conductive polycarbonate (CPC) pads are inserted between the $Se_{97}S_3$ layer and the metal electrodes in order to decrease cross sectional discontinuity of interfacial tension and viscosity at the transition from the insulating to the conductive regions along the $Se_{97}S_3$ edge. These pads prevent shear flow of $Se_{97}S_3$ during the draw, further improving its continuity and uniformity.

The preform was thermally drawn at ≈265 °C at a stress of ≈650 g mm^{-2} into a fiber containing two independent photoconducting structures flanking opposite sides of the fiber as illustrated in Figure 1b. Scanning electron microscopy (SEM) images of the fiber cross section, shown in Figure 1c, reveal the continuous $Se_{97}S_3$ layer linking the CPC pads for each of the detecting structures. After the draw, the fiber was annealed under vacuum at 150 °C for two days in order to crystalize the $Se_{97}S_3$ layers for improved conductivity.[30,32]

We characterized the fiber's electronic and optoelectronic properties under AC driving conditions. The dependence of the impedance on the driving frequency was measured on one of the detectors inside a 7-cm-long fiber using an LCR Meter (Hioki 3532-50) both in the dark and under illumination by an LED (Thorlabs, M530L2) from a distance of ≈10 cm, as shown schematically in **Figure 2**a. To explain the frequency-dependent impedance, we claim that the fiber's electronic behavior can be derived from the equivalent circuit suggested on Figure 2b, which stems from the cross sectional geometry of the fiber. The impedance Z of the circuit is given by

$$Z = 2R + 2R_{CPC}/(1 + j R_{CPC} C_{CPC} \omega) + R_{Se}/(1 + j R_{Se} C_{PSU} \omega) \quad (1)$$

R is the contact resistance and C_{PSU} is the parasitic capacitance between the electrodes. These two parameters are independent from any illumination. R_{Se} is the $Se_{97}S_3$ layer resistance, where the most significant illumination-induced change is expected to occur. R_{CPC} and C_{CPC} are the effective resistance and capacitance of the CPC pads, respectively, which include contributions from the CPC-$Se_{97}S_3$ junction that are also affected by illumination, though not as significantly. Figure 2c displays the measurement results together with the best fits from the suggested equivalent circuit. Note that while these measurements were performed with an external illumination source, we expect the photo-response to be the same for light generated inside the fiber since the optical losses of the PSU cladding are negligible over the distances considered here. The values of R and C_{PSU} resulting from the fits were found to be 4 kΩ and 7 pF, respectively. R_{CPC}, C_{CPC} and R_{Se} were found to be 498 kΩ, 1162 pF and 2031 kΩ in the dark and 422 kΩ, 950 pF and 1196 kΩ under illumination, a photo-induced change of 15%, 18% and 41%, respectively. The quality of the fits stresses that the simple equivalent circuit suggested here accurately describes the detector's optoelectronic frequency response. The optical bandwidth of this detector under a DC driving voltage and sinusoidally modulated optical source was measured to be 400 Hz, which is sufficient for recording CL signals resulting from intake of the analyte, having a typical rise time on the order of seconds.[17]

Since the impedance of the detector depends on the driving frequency, we can obtain the frequency f_{max} (SNR) at which the SNR performance of the registration setup will be optimal. We notice from Figure 2c that the ratio of impedances under illumination and in the dark $|Z_{bright}|/|Z_{dark}|$ is minimized at $f_{min}\left(|Z_{bright}|/|Z_{dark}|\right) = 2.3\,\text{kHz}$. At this frequency the photocurrent signal maximally contrasts the dark current background. Since the noise current (and thus the NEP) is strongly correlated to the dark current amplitude, the SNR is maximized at this frequency, i.e $f_{max}(\text{SNR}) = f_{min}\left(|Z_{bright}|/|Z_{dark}|\right)$. Note that the same expression for f_{max} (SNR) can be derived by explicitly considering the scaling of the noise current (see the Supporting Information). This study represents the first frequency-dependent characterization of photodetecting fibers and will be relevant for other electronic and optoelectronic fiber devices.

Adv. Mater. **2012**,
DOI: 10.1002/adma.201203053

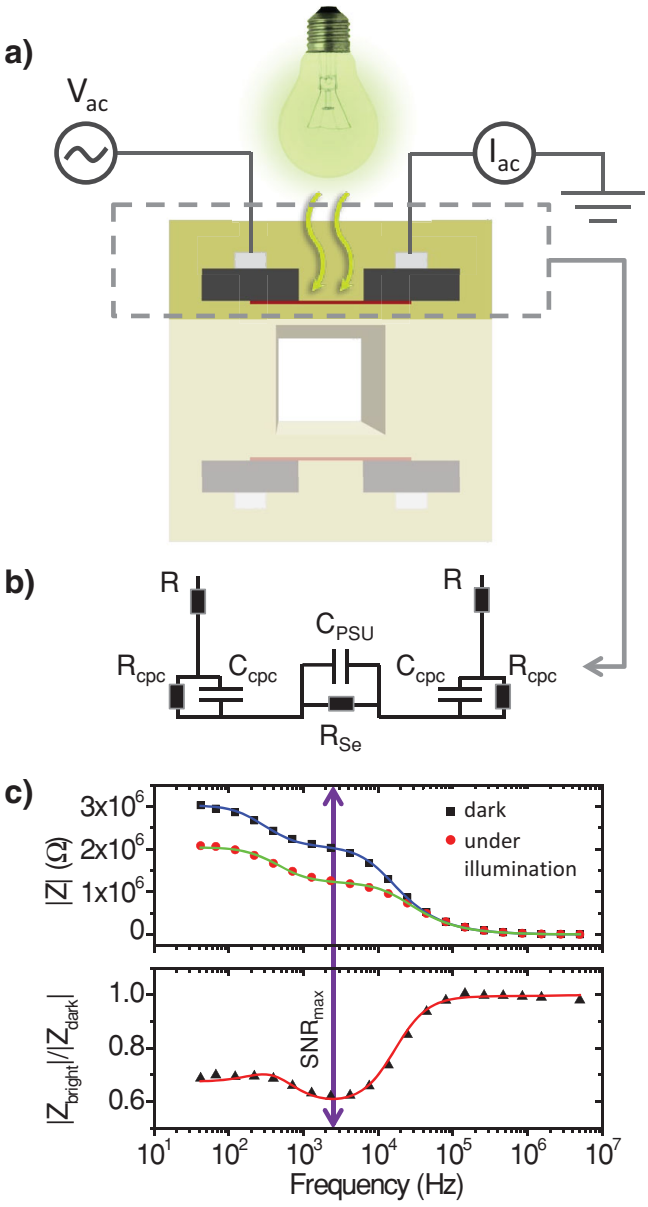

Figure 2. Characterization of the photodetecting structure: a) Schematic of the optoelectronic characterization setup used to measure the current in the dark and under illumination for one of the fiber-embedded photodetecting structures. b) Suggested equivalent circuit for the photodetecting structure. c, top) Fiber impedance frequency response (absolute value) in the dark - $|Z_{dark}|$ (black squares) and under illumination - $|Z_{bright}|$ (red circles), with the best fits of Equation 1 (blue and green curve, respectively). c, bottom) $|Z_{bright}|/|Z_{dark}|$ (black triangles) as a function of driving frequency, together with the ratio between the respective fits (red curve).

An important characteristic of this photodetector is its responsivity, which we measured by illuminating the fiber with the aforementioned LED at a known optical intensity and recording the corresponding photocurrent through one of the photodetecting structures. This measurement was performed by driving the fiber and measuring its photo-response with a lock-in amplifier (Sanford Research System, SR810) at the optimal driving frequency (2.3 kHz) under driving voltage amplitudes ranging from 0–2 V, for which the responsivity was found to be invariant when normalized to I_{dark}. Accordingly, we express the responsivity in terms of the % of I_{dark} addendum to the photocurrent per unit of optical flux through the detector area, which we found to be $r = 0.090 \pm 0.003 \left[\frac{\%\text{ of Idark}}{nW}\right]$. This normalized responsivity r translates into an actual responsivity of 0.246 nA/nW for a typical dark current of 0.273 µA used in the subsequent CL measurements. Furthermore, noise current measurements for this range of driving voltages revealed that the sensitivity of our signal registration setup is limited to 0.1 nA by the lock-in amplifier resolution rather than by the fiber detector itself.

The fiber is prepared for peroxide measurement by coating the inner surface with the sensing material[17] and hermetically sealing one end to tubing that is attached to a syringe pump. The optofluidic system and electronics setup is shown schematically in **Figure 3**a–c. A standard measurement protocol is divided into a number of stages, each labeled by a corresponding Roman numeral in Figure 3d, which depicts a typical measurement. First (I), the current in the fiber-embedded photodetector is recorded for 20 s in order to obtain the baseline. Second (II), the syringe pump is turned on at a flow rate of 50 cc/min and the fiber is purged for 30 s with air. During this phase the current slightly decreases due to the purging of the peroxide residue from the previous measurement. Third (III), the free fiber end is exposed to the headspace of a vial containing an aqueous peroxide solution of known peroxide concentration for 20 s. During this phase vapors of peroxide flow through the fiber core and interact with the sensing material which results in CL. This light is captured by the fiber-embedded photodetecting structure, and the lock-in amplifier registers the resulting photocurrent as a current addendum to the baseline. Fourth (IV), the vial is removed while the pump continues to run for an additional 20 s. Finally (V), the pump is turned off and the current gradually returns to the baseline level.

According to the protocol described above, photocurrent measurements were performed for liquid phase peroxide concentrations increasing from 1 to 35%, from which vapor phase concentrations were calculated using Henry's Law.[33] All measurements were performed at the driving frequency of 2.3 kHz while the dark current was 0.273 µA with a driving voltage of 0.5 V. The curve describing the photocurrent vs. vapor phase peroxide concentration resulting from these measurements has a slope of 0.043 ± 0.001 nA/ppm and is shown on Figure 3e together with the noise current of 0.127 nA (standard deviation over a 1 s interval). Using the detector's normalized responsivity and the above dark current, these measurements were translated into a sensitivity curve having a slope of 0.176 ± 0.005 nW/ppm with a noise level of 0.517 nW corresponding to a NEP of 0.731 nW $Hz^{-0.5}$. The detection limit at SNR = 1 was found to be 3.0 ± 0.1 ppm for this sensitivity slope and noise level.

In order to increase the performance of the all-in-fiber chemical sensor, we integrated it into a system that provides heat to the peroxide sensing material (≈80 °C) in order to obtain optimal CL efficiency and uses a peristaltic pump at a continuous flow rate of 60 cc/min for analyte vapor delivery. The electronics for this setup were limited to operation at a DC voltage, which is not the optimal condition, as was shown earlier. Measurements were performed on a 7-cm section of

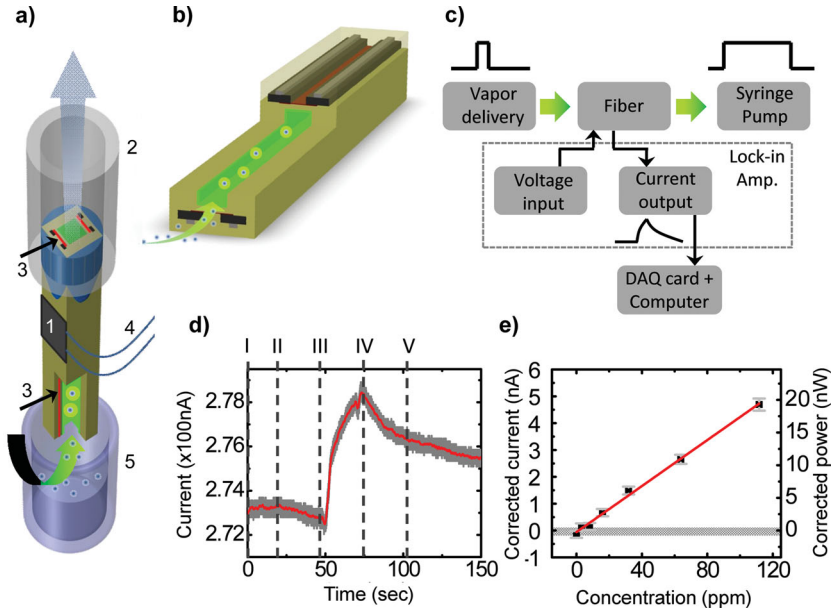

Figure 3. Chemiluminescent measurement setup and results: a) Schematic of the measurement scheme. (1) The fiber is secured into (2) an adaptor connected to the flexible tubing of the syringe pump intake. PSU cladding is locally removed to expose the electrodes connected to (3) the photodetector, and (4) external wires are connected to the individual electrodes. The fiber is inserted into (5) the headspace of the vial containing the peroxide solution. b) The fiber section schematic in greater detail. c) Block diagram of the setup. The syringe pump delivers the peroxide vapor into the fiber. The photodetecting fiber structure is driven by a voltage input from the lock-in amplifier and the result of a sensing event is registered as a current output. The signal is then recorded by a data acquisition (DAQ) card and buffered to computer. d) A typical photocurrent measurement resulting from the protocol described in the text. Raw current data (grey curve) is overlaid with the current moving average over 1 s (red curve). e) Peroxide sensitivity curve. Experimental points (black squares with error bars) are depicted with the linear fit (red solid line) and the noise level (patterned strip).

fiber with a cross section similar to the one in Figure 1c. The CL material was coated on the inner wall of a coating-stripped silica capillary (Polymicro TSP530660) of the same length as the fiber and was then inserted into the fiber's core. Five volts DC was applied across the photodetecting structures' electrodes contacted in parallel and the current was registered by an electrometer (Keithley 6517). Although heating the fiber from room temperature up to 80 °C reduced photoconductivity by a factor of three and slightly increases the noise due to a doubling of the dark current, in this configuration the photodetecting fiber was found to sense hydrogen peroxide vapor concentrations as low as 10 ppb as shown in **Figure 4**a. This detection limit is comparable to state-of-the-art commercially available systems and three orders of magnitude more sensitive than the performance depicted in Figure 3e. About an order of magnitude in this increase is attributed to the higher driving voltage and the rest arises from the enhancement in CL material sensitivity to peroxide at the elevated temperature.[21] Note that in the present measurements, a signal from water sets the detection limit. Importantly, this signal is not the result of an optical event, but arises from transient heating/cooling of the fiber when moisture-rich air from the headspace of a water-only vial passes through a heated inlet tip before entering the fiber. If eliminated, the prototype limit-of-detection would improve by another order of magnitude and would be able to measure single ppb level of peroxide vapor.

We point out several practical considerations that are relevant in the design of a remote and/or distributed chemical sensing system using these fibers. First, unlike optical transmission fibers, photodetecting fibers are not immune to electromagnetic interference. This problem can be alleviated by using standard electronic filtering techniques and/or by engineering electromagnetic barriers for blocking particular radiation from reaching the photoconductive structure.[23,34] Second, the dark current will scale linearly with fiber length if all of the chalcogenide glass is crystalized.[24] To circumvent the reduction in sensitivity associated with the increased dark current, the fiber may be selectively crystalized[30] only at those axial locations where a sensing event is expected to occur. For example, in a remote sensing application, only the last few centimeters of a fiber would need to be coated with CL material and crystalized, in which case the sensitivity would not depend on the length of the remaining fiber segment. This length independence stems from the fact that the conductivity of the in-fiber crystalized $Se_{97}S_3$ is about 8 orders of magnitude higher than in the amorphous state.[30] A particular advantage of the extended photodetecting structure is the potential for distributed sensing, such as illustrated in Figure 4b, where a periodic array of intake holes can be introduced along the fiber length for large area vapor sampling. As in the example with remote sensing, not the entire fiber but only short sections near the intake holes need to be crystalized. Moreover, the location of a peroxide vapor plume along the fiber axis could be determined by implementing this

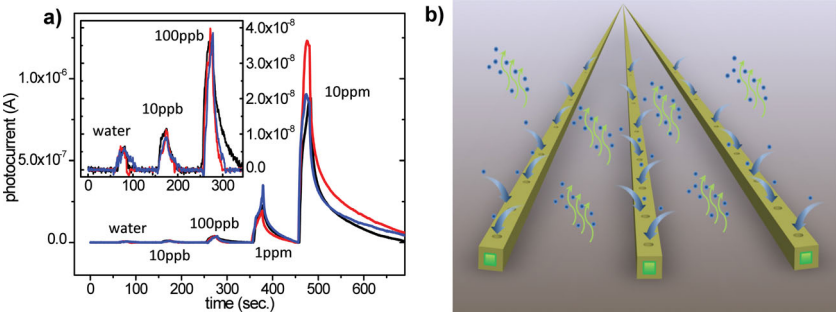

Figure 4. Improved sensitivity and vision: a) Three sensitivity measurements for a typical fiber sample. b) Concept drawing for remote and distributed sensing using hollow core photodetecting fibers. Slots can be introduced through the fiber cladding along its entire length to enable distributed, large area sample collection and measurement.

Adv. Mater. **2012**,
DOI: 10.1002/adma.201203053

distributed sensing scheme with fiber architectures having the ability to axially resolve the optical detection event along their length as described in Ref.[26]

In conclusion, we have reported the fabrication and characterization of an all-in-fiber chemical sensor for detection of trace-levels of peroxide vapor down to 10 ppb. The sensing principle is based on fiber-embedded $Se_{97}S_3$ photoconductive structures that flank a hollow core and detect CL from the reaction of a sensing material with peroxide vapor flowing through the core. These photodetecting structures can extend hundreds meters in length, suggesting possible applications for remote and distributed sensing. In principle one can further improve the NEP of the device by employing an in-fiber photodiode structure as described in Ref.[35] Furthermore, the ability to create multiple microfluidic channels in multimaterial fibers[36] paves the way towards intrafiber multianalyte detection.

Supporting Information

Supporting Information is available from the Wiley Online Library or from the author.

Acknowledgements

A.G., A.M.S., and B.R.S. contributed equally to this work. A.G. acknowledges the Yad Hanadiv fund for financial support (Rothschild fellowship). This work was supported in part by the Materials Research Science and Engineering Program of the US National Science Foundation (award no. DMR-0819762) and also in part by the US Army Research Office through the Institute for Soldier Nanotechnologies (contract no. W911NF-07-D-0004).

Received: July 26, 2012
Published online:

[1] O. S. Wolfbeis, *Anal. Chem.* **2008**, *80*, 4269.
[2] T. M. Monro, W. Belardi, K. Furusawa, J. C. Baggett, N. G. R. Broderick, D. J. Richardson, *Meas. Sci. Technol.* **2001**, *12*, 854.
[3] S. O. Konorov, A. M. Zheltikov, M. Scalora, *Opt. Express* **2005**, *13*, 3454.
[4] H. Tai, H. Tanaka, T. Yoshino, *Opt. Lett.* **1987**, *12*, 437.
[5] K. Chan, H. Ito, H. Inaba, *Appl. Opt.* **1984**, *23*, 3415.
[6] W. Jin, G. Stewart, B. Culshaw, *Sens. Actuators, B* **1997**, *38–39*, 42.
[7] J. Heo, M. Rodrigues, S. J. Saggese, G. H. Sigel Jr., *Appl. Opt.* **1991**, *30*, 3944.
[8] Y. L. Hoo, W. Jin, H. L. Ho, D. N. Wang, R. S. Windeler, *Opt. Eng.* **2002**, *41*, 8.
[9] J. Harrington, *Fiber Integr. Opt.* **2000**, *19*, 211.
[10] T. M. Monro, D. J. Richardson, P. J. Bennett, *Electron. Lett.* **1999**, *35*, 1188.
[11] T. Ritari, J. Tuominen, H. Ludvigsen, J. Petersen, T. Sørensen, T. Hansen, H. Simonsen, *Opt. Express* **2004**, *12*, 4080.
[12] A. Yildirim, M. Vural, M. Yaman, M. Bayindir, *Adv. Mater.* **2011**, *23*, 1263.
[13] T. M. Freeman, W. R. Seitz, *Anal. Chem.* **1978**, *50*, 1242.
[14] T. A. Dickinson, J. White, J. S. Kauer, *Nature* **1996**, *382*, 697.
[15] S. Smolka, M. Barth, O. Benson, *Opt. Express* **2007**, *15*, 12783.
[16] S. Afshar V., S. C. Warren-Smith, T. M. Monro, *Opt. Express* **2007**, *15*, 17891.
[17] A. M. Stolyarov, A. Gumennik, W. McDaniel, O. Shapira, B. Schell, F. Sorin, K. Kuriki, G. Benoit, A. Rose, J. D. Joannopoulos, Y. Fink, *Opt. Express* **2012**, *20*, 12407.
[18] M. S. Meaney, V. L. McGuffin, *Anal. Bioanal. Chem.* **2008**, *391*, 2557.
[19] R. Schulte-Ladbeck, M. Vogel, U. Karst, *Anal. Bioanal. Chem.* **2006**, *386*, 559.
[20] R. M. Burks, D. S. Hage, *Anal. Bioanal. Chem.* **2009**, *395*, 301.
[21] R. Deans, A. Rose, K. M. Bardon, L. F. Hancock, T. M. Swager, *Nomadics, Inc.* U. S. Patent 7799573 B2, **2010**.
[22] J. C. Sanchez, W. C. Trogler, *J. Mater. Chem.* **2008**, *18*, 5134.
[23] M. Bayindir, F. Sorin, A. F. Abouraddy, J. Viens, S. D. Hart, J. D. Joannopoulos, Y. Fink, *Nature* **2004**, *431*, 826.
[24] F. Sorin, A. F. Abouraddy, N. Orf, O. Shapira, J. Viens, J. Arnold, J. D. Joannopoulos, Y. Fink, *Adv. Mater.* **2007**, *19*, 3872.
[25] F. Sorin, O. Shapira, A. F. Abouraddy, M. Spencer, N. D. Orf, J. D. Joannopoulos, Y. Fink, *Nano Lett.* **2009**, *9*, 2630.
[26] F. Sorin, G. Lestoquoy, S. Danto, J. D. Joannopoulos, Y. Fink, *Opt. Express* **2010**, *18*, 24264.
[27] Liquid PBE were used in several terrorist acts, including: (i) The attacks on the London transit system in 2005. (see "Report into the London Terrorist Attacks on 7 July 2005" http://www.official-documents.gov.uk/document/cm67/6785/6785.pdf (last accessed September 2012)) (ii) The foiled 2006 plot to blow up several airplanes (see http://www.usnews.com/usnews/news/articles/060810/10london.htm (last accessed September 2012))
[28] A. K. Bhatnagar, K. Venugopal Reddy, V. Srivastava, *J. Phys. D: Appl. Phys.* **1985**, *18*, L149.
[29] D. S. Deng, N. D. Orf, A. F. Abouraddy, A. M. Stolyarov, J. D. Joannopoulos, H. A. Stone, Y. Fink, *Nano Lett.* **2008**, *8*, 4265.
[30] D. S. Deng, N. D. Orf, S. Danto, A. F. Abouraddy, J. D. Joannopoulos, Y. Fink, *Appl. Phys. Lett.* **2010**, *96*, 023102.
[31] E. Rosencher, B. Vinter, *Optoelectronics*, Cambridge University Press, New York **2002**.
[32] S. Danto, F. Sorin, N. D. Orf, Z. Wang, S. A. Speakman, J. D. Joannopoulos, Y. Fink, *Adv. Mater.* **2010**, *22*, 4162.
[33] J. A. Lind, G. L. Kok, *J. Geophys. Res.* **1986**, *91*, 7889.
[34] S. D. Hart, G. R. Maskaly, B. Temelkuran, P. H. Prideaux, J. D. Joannopoulos, Y. Fink, *Science* **2002**, *296*, 510.
[35] N. D. Orf, O. Shapira, F. Sorin, S. Danto, M. A. Baldo, J. D. Joannopoulos, Y. Fink, *Proc. Natl. Acad. Sci. USA* **2011**, *108*, 4743.
[36] A. M. Stolyarov, L. Wei, O. Shapira, F. Sorin, S. L. Chua, J. D. Joannopoulos, Y. Fink, *Nat. Photonics* **2012**, *6*, 229.